

What Makes Ocean Gravity Currents Flow Downhill?

Christopher C. Walker

1 Introduction

Gravity currents are the flow of one fluid through another as a result of a density contrast between the two fluids. The density contrast between the fluids can be caused by different mechanisms, for example, salinity contrasts, temperature differences, and sediment load differences. Gravity currents are common in geophysical fluid dynamics and occur on a large range of spatial and temporal scales. In the atmosphere, downslope (katabatic) winds, sea breeze fronts, and thunderstorm downdrafts are all gravity currents that are attributed to temperature differences between ambient air and cooler intruding air. Atmospheric gravity currents are also driven by differences in sediment load: avalanches and volcanic surges are both gravity currents driven by the presence of suspended particles[1].

In the ocean, gravity currents play an important role in the large-scale circulation by acting as a conduit for deep water formation. In this case, water in a marginal sea (an area of the ocean that is isolated from the rest of the ocean by topography) is subjected to sustained cooling or evaporation, and the resulting cold, dense water sinks to the bottom of the marginal sea. Once at the bottom, the dense water flows out (as a so-called “outflow”) of the marginal sea, continuing down the continental slope into the deep ocean[2].

Several models have been put forth to explain the path of oceanic outflows as they propagate down continental slopes. The simplest of these models treat outflows as frictionless, non-entraining, and steady flows. Under these conditions, geostrophic balance and the conservation of both potential vorticity and mass dictate that the current flow along a path of constant topography[3]. In this simplified model, the path and velocity of the flow are determined by the density difference between the two fluids, the slope of the incline, the Coriolis parameter, and the mass flux of the current. More complicated models of outflows, such as the streamtube models devised by Smith[4], and later extended by Price and Baringer[2], include parameterizations of bottom drag and entrainment of the ambient fluid. When friction is included in the model, the path of the current is no longer restricted to following lines of constant depth; instead, with friction present, a steady current is free to cross lines of constant depth.

Although streamtube models can be tuned to give good agreement with observations, it is clear that these models are missing some important aspects of outflows. First, streamtube models assume that the ambient fluid is quiescent, eliminating potentially important interactions between the gravity current and the surrounding fluid. Second, streamtube models are a measure of the bulk properties of the flow; no cross-stream variations are considered

in a streamtube model. Third, and most relevant to this study, streamtube models assume that the flow is steady; in a streamtube model the flux in the outflow is assumed to be constant in time.

More complicated numerical models of oceanic outflows have recently been applied to address some of the shortcomings of streamtube models. Jungclaus and Backhaus[5] developed a hydrostatic, reduced gravity, two-dimensional primitive equation model and applied it to a study of the Denmark Strait outflow. They demonstrated that the presence of bottom topography can cause complicated cross-stream variations in the flow. Subsequent numerical studies by Jiang and Garwood[6, 7] considered outflows in the context of a three dimensional ocean model. Their results revealed that the three dimensional aspects play an important role in the dynamics of the outflow. Specifically, they showed that the outflow plume can separate into smaller sub-plumes, and that as the plume propagates it can manifest itself as coherent vortices in the ambient fluid. This behavior was later observed and explored in laboratory experiments[8, 9].

In contrast with outflows, turbidity currents are an example of a transient oceanic gravity current. Turbidity currents arise when sediment on the continental slope is dislodged, often by an underwater earthquake. Once dislodged, the sediment is brought into suspension, increasing the density of the fluid in the immediate vicinity of the earthquake. This dense fluid then flows down the continental slope, entraining more sediment as it travels. The turbidity current eventually encounters a decreasing slope, slowing the current and allowing the suspended particles to settle. Large-scale turbidity currents have not been directly observed. There is, however, one turbidity current that gives a unique set of data for analysis. In 1929, an underwater earthquake occurred under the Grand Banks of Newfoundland, causing a large turbidity current that flowed down the continental slope. As this current traveled, it broke a succession of telegraph cables, each of which had a known location. The time of each breakage was also well known, giving a measure of the current's speed[10]. Subsequent investigation determined the extent of the turbidite (the material deposited by the current), providing data about the path that the turbidity current traveled down the continental slope. The turbidite indicates that the turbidity current veered to the right as it flowed, possibly under the influence of the Coriolis force.

The outflow models discussed above all model oceanic gravity currents as steady flows. While steady flow is a reasonable assumption for outflows, it is not a reasonable assumption for turbidity currents, which are a much more transient event. The only work that we are aware of that studies the effect of rotation on turbidity currents is a study by Nof[10] (hereafter referred to as Nof), which proposes a simple model (discussed more in section 4.1) of the turbidity current that resulted from the 1929 Grand Banks earthquake. Nof's model was intended to explain a slowing down of the current that was seen in the cable breakage data. As the turbidity current propagated down the continental slope, its downhill velocity decreased. Previous work attributed this slowing to a combination of three causes. First, as the current propagated, it experienced a decrease in slope which acted to slow the current. Second, as the current slowed, sediment settled out of solution and decreased the density contrast between the plume and the ambient fluid. Third, bottom friction between the slope and the plume acted to slow the plume. Nof proposed that in addition to the reasons listed above, the influence of the Coriolis force could have contributed to the decrease in downhill velocity by causing the current to veer to its right. To determine the

effect of the Coriolis force on the turbidity current, Nof modeled the turbidity current as a frictionless “blob” of fluid on a parabolic bottom. The solution to Nof’s model is a cycloid with a mean path parallel to the slope, showing qualitatively that the Coriolis force may have played a substantial role in reducing the current’s downhill speed.

This work has two goals. First, it is designed as a modeling complement to Nof’s analytic study on the role of rotation in the path of turbidity currents. Second, we wish to address the question, “If, as predicted by streamtube models, an inviscid and geostrophic gravity current propagates along contours of constant topography, under what conditions will a gravity current flow downhill?”

An outline of this paper is as follows: In section two, we outline the approach that we use to address the question raised above. In section three, we discuss a simple outflow model that is based on Smith’s streamtube model. Section three also includes comparisons of our model results with the streamtube theory. In section four, we review the model proposed by Nof[10] to explain the path of the 1929 Grand Banks turbidity current and discuss the results of our model of a turbidity current. Section five summarizes our results and answers the question raised above about the paths of oceanic gravity currents.

2 Approach

To address the question of when gravity currents flow downhill, we start by considering the horizontal momentum equation in natural coordinates (t is the unit vector parallel to the flow, n is the unit vector normal to the flow). When the flow is in steady state, it is parallel to height contours and the velocity satisfies[11]:

$$\frac{V^2}{R} + fV + \frac{\partial\Phi}{\partial n} = \frac{C_d}{H}V^2 \quad (1)$$

where V is the horizontal velocity, R is the radius of curvature of the flow, f is the Coriolis parameter, H is the height of the Ekman layer (assumed to have a maximum value of 10 m), C_d is a dimensionless bottom friction parameter, and Φ is the geopotential. The term on the right represents a height dependent boundary layer friction, so that equation (1) can be thought of as representing the momentum balance in an inviscid layer of fluid with a frictional bottom boundary layer of height H , where H has a maximum value of 10 m. For large scale flows, the term in the momentum equation representing the centrifugal force ($\frac{V^2}{R}$) is relatively small and can be neglected. When the centrifugal term is neglected and boundary layer friction is ignored, the motion is a balance between the Coriolis force and the pressure gradient force, so that the motion is geostrophic:

$$V_g = -\frac{R}{f} \frac{\partial\Phi}{\partial n} \quad (2)$$

where V_g is the geostrophic velocity. Although the geostrophic approximation is appropriate for most large-scale flows, there are regimes in which the centrifugal force cannot be neglected. In these cases, the full momentum equation (1) must be considered. The Rossby number, the ratio of the centrifugal term to the Coriolis term, gives the degree of

appropriateness of the geostrophic approximation:

$$R_o = \frac{V}{fL} \quad (3)$$

Flows with a low ($\ll 1$) Rossby number can be considered geostrophic; flows with a Rossby number near 1 must consider the full momentum equations. Another important dimensionless number is the Ekman number, which measures the relative importance of the friction term against the Coriolis term. In this case, the Ekman number is given by:

$$E_k = \frac{C_d V}{fH} \quad (4)$$

The Ekman number indicates the extent to which friction plays a role in the flow.

As mentioned in the introduction, a gravity current that is both inviscid and geostrophic will travel along a path that follows bottom topography. If a gravity current is to flow downhill, then one of these conditions must be relaxed. In this study, we use a simplified version of an ocean general circulation model to investigate situations under which these two approximations—inviscid flow and geostrophy—are no longer applicable.

We consider two flow regimes. First, a regime in which the flow is approximately in geostrophic balance, but is modified by bottom boundary friction. This describes the conditions associated with a midlatitude ($f = 10^{-4} \text{ s}^{-1}$) outflow, since the velocities of an outflow are relatively small ($\approx 40 \text{ cm s}^{-1}$) and the length scales are large ($\approx 40 \text{ km}$), giving a Rossby number on the order of 0.1. The same scales, together with a layer height of 10 m and $C_d = 0.005$, give an Ekman number of approximately 0.5, indicating that friction will play a substantial role in the motion of the plume. We also consider the behavior of an overflow at lower latitudes ($f = 5 \times 10^{-5} \text{ s}^{-1}$, $f = 10^{-5} \text{ s}^{-1}$ and $f = 0 \text{ s}^{-1}$), so that we have flows with Rossby numbers from $R_o = \infty$ to $R_o = 0.1$.

The second regime that we study is a regime in which the full equation (1) must be considered. This regime describes our model of a turbidity current, since the velocities are large ($\approx 10 \text{ m s}^{-1}$), the height H is 10 m, and the length scales are on the order of 200 km. These scalings give a Rossby number of 0.5 and an Ekman number of 50, indicating that all of the terms in (1) will play a significant role in the motion of the current.

2.1 Methods

To consider the two regimes described above, we use the Miami Isopycnal Coordinate Ocean Model (MICOM) to simulate some basic aspects of oceanic gravity currents. A full description of MICOM is beyond the scope of this work; a complete discussion of MICOM can be found in Haidvogel and Beckmann[12] and references therein. MICOM is a three-dimensional ocean model with potential density as the vertical coordinate. To study gravity currents, we run the model in a two-layer configuration: one layer representing the upper ambient fluid and a heavier layer representing the intruding gravity current. We run the model without entrainment, so that the mass in each layer remains constant.

To isolate fundamental processes in the dynamics of gravity currents, we consider two simple model configurations, one configuration designed to study outflows, and the other designed to study turbidity currents. In both configurations, we consider the motion of a plume on an f -plane.

To study outflows, we set up the model in a configuration similar to Jungclauss and Backhaus, i.e. a 320×320 km model domain with a 2 km horizontal resolution. Heavy fluid ($\Delta\rho/\rho = 2.9 \times 10^{-4}$) is released at the top of the slope, and the model is integrated for five model days. To test the dependence of the solution on the initial conditions, we release the fluid in two different manners: a “dambreak” configuration in which the heavy fluid starts as a bay (horizontal size of 30×30 km, 100 m height) of fluid at the top of the slope and is allowed to evolve with no subsequent addition of fluid. In addition to the dambreak release, we also release fluid as a constant flux at the top of the slope. There is little qualitative difference in the behavior of the plume in between the two cases; accordingly, only the results from the constant flux configuration are discussed here.

Our second configuration is designed to test Nof’s model of turbidity currents (discussed in section 4.1). Because the spatial scales of turbidity currents are large, we consider a 1000×1000 km model domain, with a 5 km horizontal resolution. Rather than release dense fluid at the top of the slope as we did in the outflow configuration, we initialize the model with a Gaussian blob (radius ≈ 100 km, maximum height of 15 m) of dense fluid ($\Delta\rho/\rho = 0.03$) near the top of the slope. Initializing the model in this manner is based on the approach taken by Nof. To make the study of turbidity currents mathematically tractable, Nof assumes that the early behavior of the turbidity current is not important to its path. Accordingly, Nof considers the fate of a geostrophically adjusted “blob” of fluid on a slope, which is taken to represent the turbidity current after the complex initial stages. To facilitate comparison with Nof’s theory, we take the same approach, although we also considered the behavior of a turbidity current starting from a dambreak configuration. We found little difference between the two initial configurations and therefore report only the results obtained with the Gaussian blob configuration.

3 Outflow regime

3.1 Limiting case of Smith’s streamtube model

In the streamtube model formulated by Smith[13, 4], the outflow is treated as a steady flow on a simple linear slope. The streamtube model starts with the hydrostatic, incompressible Navier-Stokes equations and considers the cross-stream properties of a “tube” of fluid¹. With the simplifying assumptions made by Smith, and by neglecting entrainment into the plume and stratification of the ambient fluid, the motion of the flow can be reduced to a set of two ordinary differential equations:

$$V(f + V \frac{d\beta}{d\xi}) = g' \alpha \cos \beta \tag{5}$$

$$\frac{d(AV^2)}{d\xi} = g' \alpha A \sin \beta - C_d W V^2 \tag{6}$$

where ξ is a coordinate that is along the path of the flow, α is the slope of the topography, β is the angle that the streamtube makes with a line running parallel to topography, V is the mean velocity of the flow, $A = HW$ is the cross-sectional area of the flow, where H

¹The details and derivation of the streamtube model can be found in [13]

and W are the height and width of the streamtube, respectively, and C_d is a parameter taken to represent friction from bottom drag. Note that C_d has the same meaning as it has in equation (1), and that it has been multiplied by the width of the plume because of the cross-stream integration performed as part of the streamtube analysis.

When the full streamtube equations are integrated numerically, the motion of the plume is initially a cycloid with a mean path along the slope. Far downstream, friction damps out any cyclic component of the flow, and the flow settles into a steady state such that $\frac{d}{d\xi} = 0$. At this limit, equations (5) and (6) can be combined to give:

$$\tan \beta = \frac{C_d V}{f H} \quad (7)$$

$$\left(\frac{C_d}{H f}\right)^2 V^4 + V^2 = \left(\frac{g' \alpha}{f}\right)^2 \quad (8)$$

Note that the above expression for $\tan \beta$ is similar to the expression for the Ekman number (4). The only difference between the two expressions is that in the definition of the Ekman number, H corresponds to the height of the mixed layer and therefore has a maximum value of 10 m. In equation (7), H is the height of the streamtube, with no maximum value (although the height of the flow is generally less than 100 m). In spite of this difference, we refer to the right hand side of equation (7) as the Ekman number (E_k). As defined above, β is the angle that the streamtube makes with a line running along the topography. The expression for $\tan \beta$ is therefore the ratio of the velocity across the topography to the velocity along the topography, or

$$\tan \beta = E_k = \frac{V_{across}}{V_{along}} \quad (9)$$

The solution to equations (7) and (8) is most useful when it is written in terms of external variables so that the path and velocity of the streamtube can be predicted. As in Price and Baringer[2], we assume that the width of the plume is constant so that the volume flux per unit width, Q , is written as $Q = VH$. Substituting this expression into equations (7) and (8) gives:

$$\tan \beta = \frac{C_d V^2}{f Q} \quad (10)$$

$$\left(\frac{C_d}{Q f}\right)^2 V^6 + V^2 = \left(\frac{g' \alpha}{f}\right)^2 \quad (11)$$

3.2 Comparison with model results

We consider two methods of solving equations (10) and (11), which we designate Method 1 and Method 2. Each method has an associated velocity (which we denote as V_1 and V_2), and an associated β (β_1 and β_2).

The first method, Method 1, considers the simultaneous solution to equations (10) and (11). The solution to equation (11) has only one positive real root (V_1), which is substituted in (10) to obtain β_1 .

The second method of solving equations (10) and (11)—the approach taken by Price and Baringer[2]—is to assume that the flow is in geostrophic balance. Method 2 does not make use of the predictive expression for the velocity, equation (11); instead, it assumes that the velocity, V_2 , is given by geostrophic velocity, U . The geostrophic velocity for flow on a constant linear slope is given by

$$V_2 = U = \frac{g'\alpha}{f} \quad (12)$$

When (12) is substituted into (10), the following expression results:

$$\tan \beta_2 = \frac{C_d(\alpha g')^2}{Qf^3} \quad (13)$$

To test the predictive capabilities of the two methods of solving the streamtube equations and to observe the sensitivity of the outflow path to different parameters, we integrated the model with different rotation rates and different values of bottom friction. The path of the outflow for different rotation rates is seen in Fig. 1, which shows the height (thin contours) of the plume² on day five of the integration, for four different rotation rates. Each panel in Fig. 1 also shows the path predicted by the two different methods of solving the streamtube equations. Method 1, which is the simultaneous solution to equations (10) and (11), is shown as a heavy solid line. Method 2, which assumes that the plume is in geostrophic balance, is shown as a heavy dashed line. Dense fluid is released at a constant flux (per unit width) of $20 \text{ m}^2 \text{ s}^{-1}$ near the top right corner of each panel between 210 km and 240 km. To avoid the complications associated with flow near a boundary, the fluid is released on the slope 20 km from the top edge of the domain. The topography starts at the top of each panel with a value of -500 m and declines linearly towards the bottom of each panel. In each case, the slope of the topography is 0.008 and bottom friction (C_d) is 0.01. The rotation rate has values of 0 s^{-1} (upper left panel), 10^{-5} s^{-1} (upper right panel), $5 \times 10^{-5} \text{ s}^{-1}$ (lower left panel), and 10^{-4} s^{-1} (lower right panel). As a complement to Fig. 1, Table 1 shows the values of velocity³ and Ekman number ($\tan \beta$) obtained by the two different solution methods for the integrations shown in Fig. 1. Table 1 also shows the measured average velocity of the plume, where we define the average velocity of the plume as the instantaneous average velocity of all points that have a thickness of 10 m or more.

The effect of rotation is seen clearly in Fig. 1: as the rotation rate is increased, the path of the outflow is increasingly to the right (northern hemisphere configuration). For the case without rotation, the path is directly downhill. When the rotation rate is 10^{-4} s^{-1} , which corresponds to a latitude of approximately 45° , the path is substantially deflected.

With some notable exceptions, the predictions given by the streamtube theory are in good agreement with the model results. Without rotation, the behavior of the streamtube equations is pathological because of the presence of f in the denominator in equations (10) and (11). In the limit of very small f , however, the simultaneous solution to equations (10) and (11) (Method 1) gives a velocity of approximately 42.4 cm s^{-1} and a very large $\tan \beta$. These values are in accord with the measured velocity, 40.1 cm s^{-1} , and an infinite $\tan \beta$. Method 2 is not applicable without rotation, since the geostrophic velocity approaches infinity as f approaches 0.

²We define the plume as the dense fluid with a height of 10 m or greater.

³Note that the table entry for $f = 0 \text{ s}^{-1}$ is the solution to (10) and (11) as $f \rightarrow 0$

	Method 1		Method 2		Observed
	V_1 (cm s ⁻¹)	$\tan \beta_1$	V_2 (cm s ⁻¹)	$\tan \beta_2$	V (cm s ⁻¹)
$f=0$ s ⁻¹	42.4	∞	∞	∞	40.1
$f=10^{-5}$ s ⁻¹	42.3	9.0	381.6	728.2	40.0
$f=5 \times 10^{-5}$ s ⁻¹	40.2	1.61	76.3	5.83	37.5
$f=10^{-4}$ s ⁻¹	33.4	0.56	38.2	0.73	32.7

Table 1: Velocity and $\tan \beta$ for the experiments in Fig. 1 for the two different methods of solving the streamtube equations.

	Method 1		Method 2		Observed
	V_1 (cm s ⁻¹)	$\tan \beta_1$	V_2 (cm s ⁻¹)	$\tan \beta_2$	V (cm s ⁻¹)
$C_d=0.001$	38.1	0.07	38.2	0.07	43.1
$C_d=0.005$	36.3	0.32	38.2	0.36	37.5
$C_d=0.01$	33.4	0.56	38.2	0.73	32.7
$C_d=0.05$	23.0	1.32	38.2	3.64	19.1

Table 2: Velocity and $\tan \beta$ for the experiments in Fig. 2 for the two different methods of solving the streamtube equations.

In all cases with rotation, the path predicted by Method 1 agrees well with the modeled plume. For $f = 5 \times 10^{-5}$ s⁻¹, for example, the angle predicted by Method 1 is close to the angle of center of the plume, and the predicted velocity, 40.2 cm s⁻¹, is close to the measured value of 37.5 cm s⁻¹. Similar agreement is found in all cases with rotation.

In contrast with the predictions by Method 1, the agreement between the path predicted with Method 2 and the modeled plume depends on the rotation rate. The path predicted by Method 2 agrees well at the highest rotation rate, $f = 10^{-4}$ s⁻¹, but diverges from the model at lower rotation rates. This discrepancy exists because the flow is not in geostrophic balance. Method 2 assumes that the flow is in geostrophic balance; consequently, considering the Rossby number of the flow will give an indication of the appropriateness of Method 2. Using the same scalings as used in section 2 (length \approx 40 km, velocity \approx 40 cm s⁻¹), for $f = 10^{-5}$ s⁻¹, $f = 5 \times 10^{-5}$ s⁻¹, and $f = 10^{-4}$ s⁻¹, the Rossby number is 5, 1, and 0.1, respectively. These values of the Rossby number indicate that Method 2 is not appropriate for $f = 10^{-5}$ s⁻¹ and $f = 5 \times 10^{-5}$ s⁻¹. This is also apparent in a comparison between the geostrophic velocity and the observed velocity. For the case of $f = 5 \times 10^{-5}$ s⁻¹, for example, the measured velocity of the plume is 37.5 cm s⁻¹, while the geostrophic velocity is 76.3 cm s⁻¹.

We also examined the impact of bottom friction on the outflow's path. Figure 2 shows the height of the intruding current and the path predicted by the streamtube model for the two different solution methods, on day five of the integration, for four different values of bottom friction. The experimental setup is identical to that used to produce Fig. 1, except that in this case, the rotation rate is held constant at 10^{-4} s⁻¹ and the bottom friction coefficient is varied. The panels in Fig. 2 show the outflow path that results with bottom friction values of 0.001 (upper left panel), 0.005 (upper right panel), 0.01 (lower left panel), and 0.05 (lower right panel). For comparison, typical values of bottom friction used in ocean

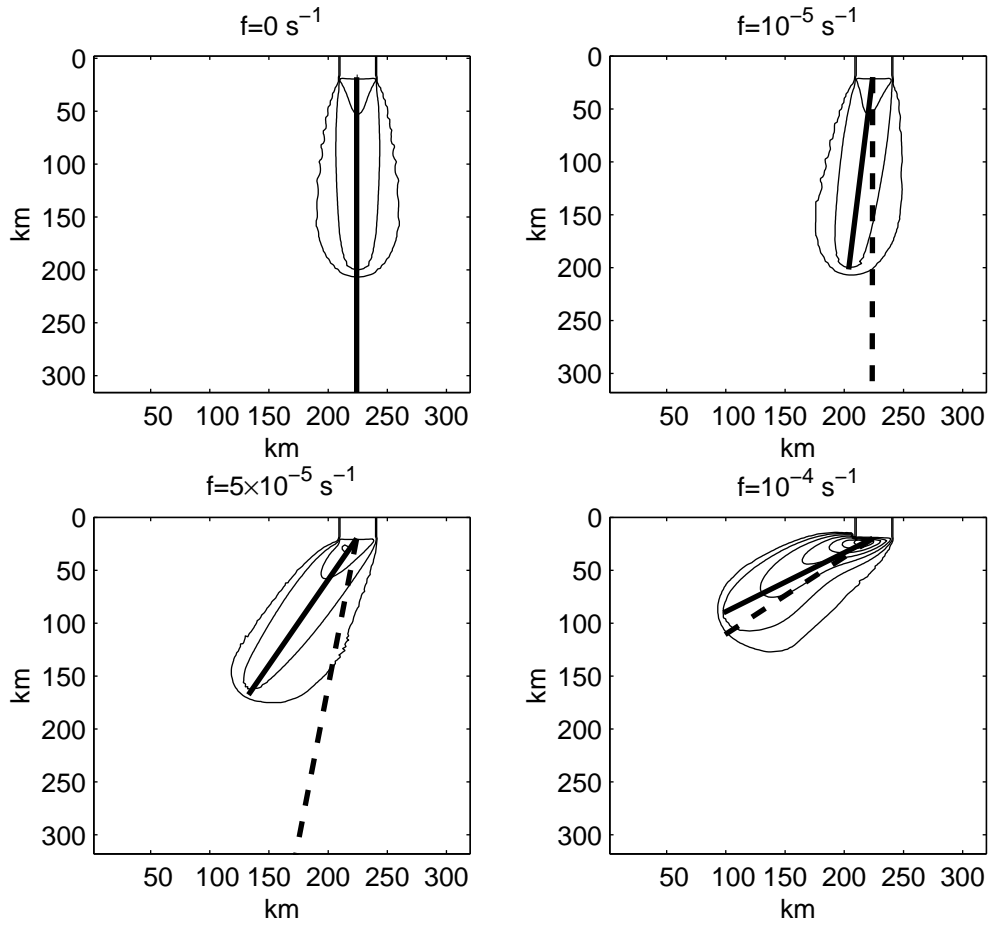


Figure 1: Plume height (thin contours) and path predicted by streamtube theory with Method 1 (thick solid line) and Method 2 (thick dashed line), on day 5 for different rotation rates: 0.0 s^{-1} , 10^{-5} s^{-1} (top right), $5 \times 10^{-5} \text{ s}^{-1}$ (bottom left), 10^{-4} s^{-1} (bottom right) for a slope of 0.008 and a bottom drag (C_d) of 0.01. Contour interval is 10 m.

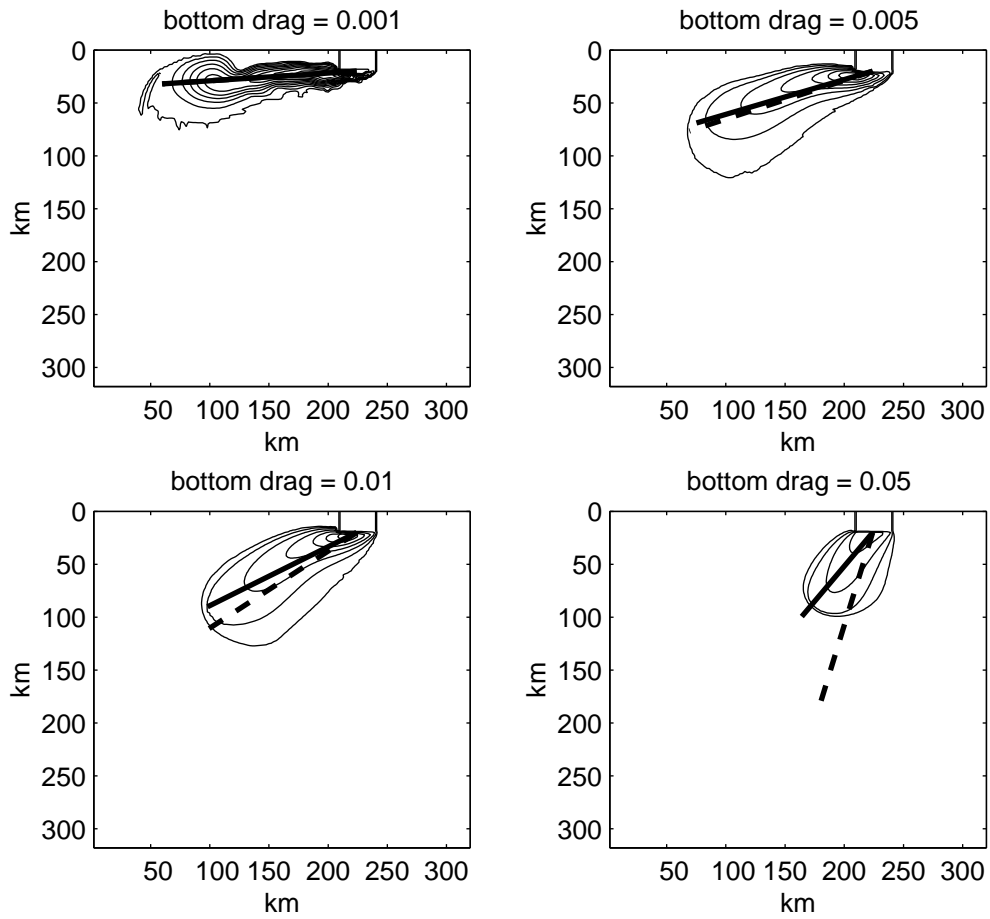


Figure 2: Plume height (thin contours) and path predicted by streamtube theory with Method 1 (thick solid line) and Method 2 (thick dashed line), on day 5 for different values of bottom drag (C_d): 0.001 (top left), 0.005 (top right), 0.01 (bottom left), 0.05 (bottom right) for a slope of 0.008 and a rotation rate of 10^{-4} s^{-1} . Contour interval is 10 m.

modeling are around 0.003. It is clear from Fig. 2 that as bottom friction is increased, the gravity plume is able to cross lines of constant depth with an increasingly steep angle. For the smallest value of bottom friction, 0.001, the flow is almost parallel to topography. This is consistent with the simplest (i.e. inviscid) models of outflows that predict alongslope flow.

In all cases, there is reasonably good agreement between the path of the model and the path predicted by the two methods of solving the streamtube equations. For lower values of bottom friction, $C_d=0.001$ and $C_d=0.005$, the two methods give very similar predictions. This is seen in Table 2, which shows the velocity and Ekman number predicted by the two solution methods and the observed velocity of the plume for the cases shown in Fig. 2. For example, the velocities predicted by Method 1 and Method 2 for the case when bottom friction is 0.005 are 36.3 cm s^{-1} and 37.5 cm s^{-1} , respectively.

At higher values of bottom friction ($C_d=0.01$ and $C_d=0.05$), the path predicted by Method 2 is more downhill than the path predicted by Method 1. This is due to the decelerating influence of friction, which prevents the plume from achieving geostrophic balance. At higher values of friction, the measured velocity is substantially less than the geostrophic velocity. For example, when bottom friction is 0.05, the measured velocity of the plume is approximately 19.0 cm s^{-1} , while the geostrophic velocity is 38.2 cm s^{-1} . The velocity predicted by Method 1 adjusts to the higher value of friction, resulting in a more accurate prediction of the plume's path.

One can also apply the streamtube model in a local sense by considering each point in the domain as an individual streamtube with its own mass flux. In this case, the velocity and height of the flow are diagnosed at each grid point, and these fields are substituted into equation (7). The resulting field gives information about the path that is preferred locally, in contrast with the bulk streamtube which gives the preferred path of the bulk plume. Figure 3 shows the 'local streamtube' field (arrows)⁴ for the case when bottom friction is 0.005 (the same case shown in the upper right panel of Fig. 2). Also shown in Fig. 3 are the predictions by the two different methods of solving the streamtube equations. Near the center of the plume, the local streamtube field is oriented in a direction nearly parallel to the bulk streamtube approximation. Away from the center of the plume, however, the height of the plume tends to decrease, resulting in a corresponding decrease in the local mass flux. The decrease in the local mass flux causes the local streamtube field to diverge from the direction predicted for the bulk plume. Price and Baringer[2] suggest that bottom friction might play a role in the spreading of outflows. Figure 3 suggests a mechanism through which this spreading might occur: as fluid moves away from the center of the plume, the local Ekman number of the flow rises, indicating an increase in the relative importance of friction. The increase facilitates the downhill motion of the fluid, leading to a spreading of the outflow.

⁴Note that the field plotted in Fig. 3 is normalized so that the length of each arrow is 1; the length of the arrows does not indicate the magnitude of the local Ekman number, only the direction that the local Ekman number predicts for the flow

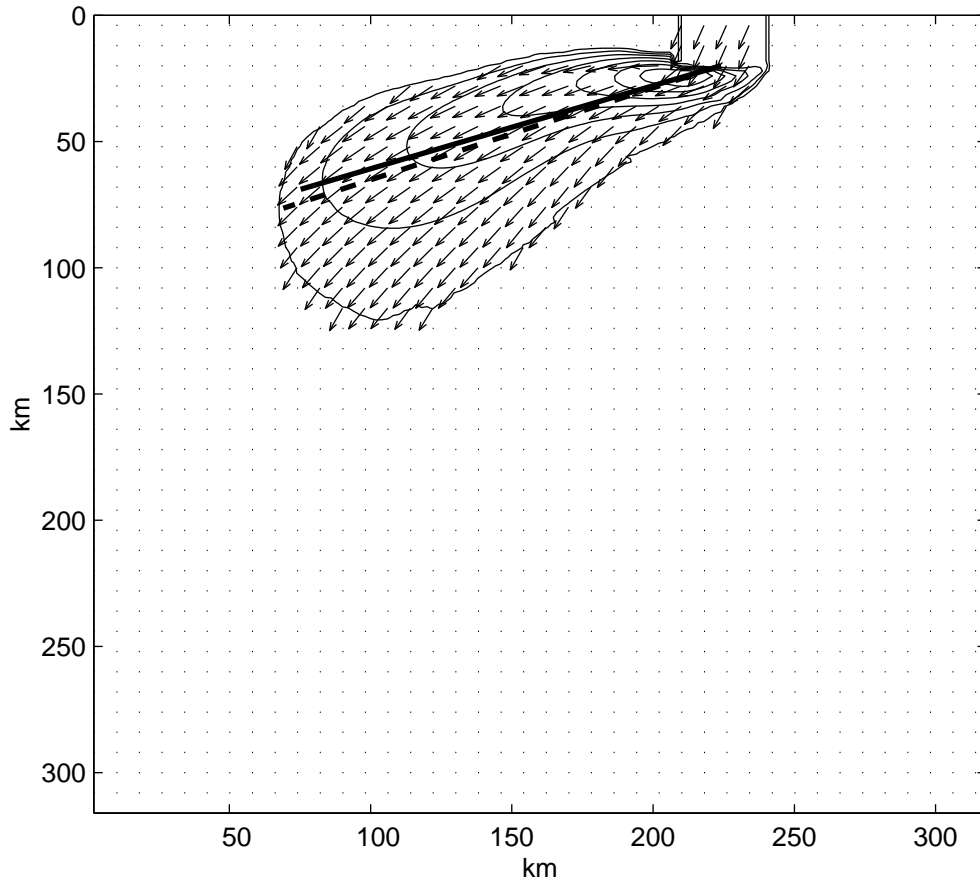


Figure 3: Thickness (thin contours—interval 10 m), bulk streamtube model (Method 1—thick solid line; Method 2—thick dashed line), and local streamtube (arrows), on day 5 of integration for a bottom drag value of 0.005

4 Turbidity current

4.1 Nof’s (1996) turbidity current theory

Nof proposes a simple analytic model to explain the path of the turbidity current associated with the 1929 Grand Banks earthquake. Rather than consider the complex processes that lead to the formation of the turbidity current, Nof simplifies the problem by treating the turbidity current as a geostrophically adjusted “blob” of fluid on parabolic slope. Nof makes further simplifications by treating the shape of the blob as constant in time and by neglecting the effect of viscosity and bottom drag. For brevity, we only present the solution; for the derivation of Nof’s model, see Nof (1996).

With the simplifications discussed above, the motion of the blob of fluid is given by the following two components:

$$X(t) = \frac{-g'T_1 f}{(f^2 + 2g'T_2)^{\frac{3}{2}}} ([f^2 + 2g'T_2]^{\frac{1}{2}} t - \sin[(f^2 + 2g'T_2)^{\frac{1}{2}} t]) \quad (14)$$

$$Y(t) = \frac{-g'T_1}{(f^2 + 2g'T_2)} (1 - \cos[(f^2 + 2g'T_2)^{\frac{1}{2}} t]) \quad (15)$$

where X and Y are position of the center of the blob as a function of time, t , $g' = g \frac{\Delta\rho}{\rho}$ is the reduced gravity, f is the Coriolis parameter, and the constants T_1 and T_2 describe the parabolic topography, such that the topographical height can be written as $z = T_1 y + T_2 y^2$ (in all cases considered below, $T_2 = 0$).

4.2 Comparison between Nof’s theory and model results

To test Nof’s theory of the 1929 Grand Banks earthquake and to investigate flow with a relatively high Rossby number, we integrated the model in the turbidity current configuration described in section 2. We considered the evolution of a Gaussian “blob” of fluid with a radius of approximately 100 km and a maximum height of 150 m on linear topography with a slope of 0.006 (similar values to those considered in Nof) over a two day period. Figure 4 shows the height of the blob every 6 hours (thin contours) over the first day of integration and the path predicted by Nof’s theory (thick line) for the center of the blob. Figure 4 also shows, as a heavy red contour (stippled in black and white), the regions where the Rossby number⁵ is larger than 1. The beginning Nof’s theory (around $X = 600$ km, $Y = 180$ km) marks the center of the blob at $t = 0$. For the first 6 hours (upper left panel in Fig. 4), the blob roughly follows the path predicted by Nof’s theory, deflecting to the blob’s right under the influence of the Coriolis force. After the first 6 hours, however, the blob’s path diverges substantially from Nof’s theory. Note that in contrast with Nof’s theory, which assumes that the blob maintains its shape, the blob has deformed substantially during this interval.

At 12 hours (upper right panel in Fig. 4), the fluid that was initially in the blob begins to collect in a region (around $X = 400$ km, $Y = 550$ km) that is characterized by high velocities (~ 6 - 10 m s⁻¹). This rapidly moving region, which we call “the drip” region, grows throughout the rest of the simulation, such that by the end of the first day (lower

⁵To calculate the Rossby number, we define the length scale as 75 km, approximately the radius of the initial Gaussian plume

right panel in Fig. 4), most of the fluid that was present in the initial Gaussian blob is in the drip region. The velocities in the drip region are large enough that the nonlinear terms in equation (1) become important. The importance of the nonlinear terms can be seen by looking at the local Rossby number. At 6 hours into the simulation (upper left panel), the Rossby number is larger than 1 (maximum value of approximately 1.6) towards the bottom right-hand side (towards $x=0$, $y=1000$) of the blob. As the simulation proceeds, the drip region forms in the area where the Rossby number is greater than 1, indicating the importance of non-linear terms in the formation of the drip region.

Figure 5 shows the height of the blob (thin contours) and the path predicted by Nof's theory (thick line) for a case that is identical to the case shown in Fig. 4, but with topographical slope of 0.003, half of the value used in the simulation shown in Fig. 4. In this case, a drip region does not form. In addition, the blob of heavy fluid follows Nof's theory for a longer time; the blob's path agrees reasonably well with the theory for approximately 12 hours. In this case, the Rossby number of the flow (not visible), calculated in the same manner as in Fig. 4, never exceeds 1. Instead, the Rossby number of the flow has a maximum value of approximately 0.75. It is interesting to note that if this same case is considered with a smaller value of bottom friction, shown in Fig. 6, the Rossby number of the flow does exceed 1, and, on day one, the flow begins to develop a drip region similar to that shown in Fig. 4.

5 Conclusion

In an effort to understand the processes that allow an oceanic gravity current to flow downhill, we have modeled gravity currents in two different flow regimes. First, we considered the motion of outflows, which in the midlatitudes are approximately in geostrophic balance but are modified by the presence of friction. The simplest available model—the bulk streamtube model—predicts that the presence of friction will allow the outflow to propagate downhill. Our dynamical model of an outflow is consistent with the simple streamtube model: as we increase bottom friction, the motion of the outflow is increasingly downhill. We also extended the streamtube model so that it can be applied in a local sense. Applying the streamtube model in this manner gives information about how an outflow plume spreads as it travels.

The second flow regime that we considered is the flow of a turbidity current. In this case, the velocities associated with the motion are high enough ($\sim 10 \text{ m s}^{-1}$) that the motion cannot be described by the geostrophic approximation. We compared the motion of a Gaussian blob of fluid, taken to represent a turbidity current after the initial formation stages, with the motion predicted by Nof's theory of turbidity currents. We found that for an initial period, around 6 hours, the motion of the blob was close to the Nof's theory. After this initial period, however, the blob of fluid diverged from the cycloid motion predicted by Nof. The difference between Nof's theory and the model is likely due to two factors. First, Nof's theory assumes that the blob does not change shape as it propagates. This is a severe restriction, imposed to simplify the mathematics. Our model does not impose any restrictions on the evolution of the blob's shape; indeed, as shown in the Fig. 4, the shape of the plume changes dramatically in time. Second, Nof's model assumes that there is no bottom friction and that the flow is inviscid. For reasons of numerical stability, we are not

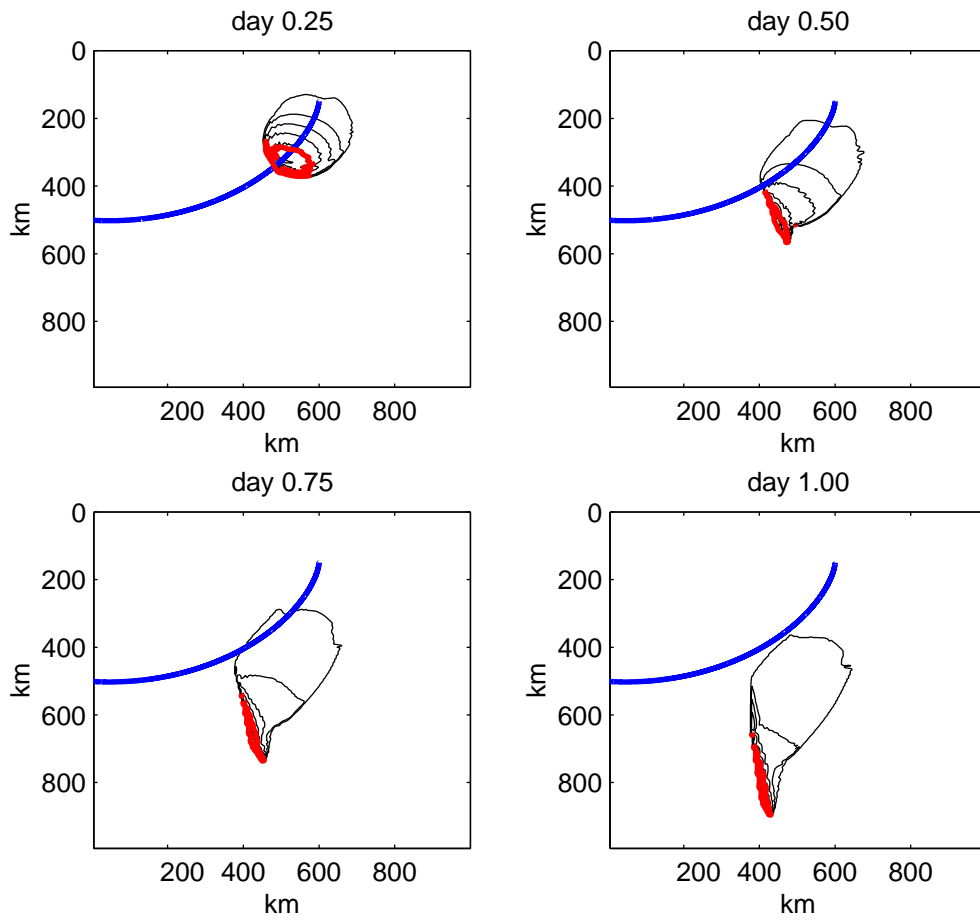


Figure 4: Thickness (contours) and Nof theory (heavy blue line) for day 0.25 (top left), day 0.5 (top right), day 0.75 (bottom left), and day 1.00 (bottom right) of turbidity current simulation with slope 0.006 and $f=10^{-4} \text{ s}^{-1}$. Areas with Rossby number greater than 1 are shown with a heavy red contour (stippled in black and white). Height contour interval is 10 m.

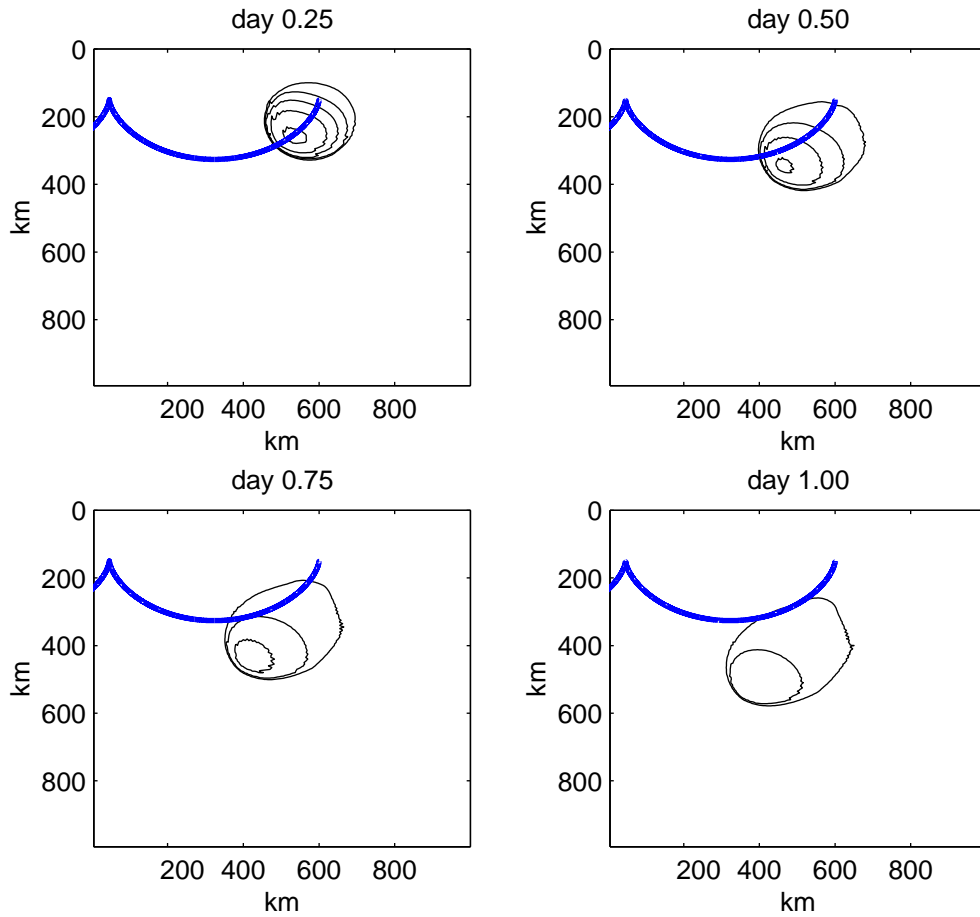


Figure 5: Thickness (contours) and Nof theory (heavy blue line) for day 0.25 (top left), day 0.5 (top right), day 0.75 (bottom left), and day 1.00 (bottom right) of turbidity current simulation with slope 0.003 and $f=10^{-4} \text{ s}^{-1}$. Contour interval is 10 m.

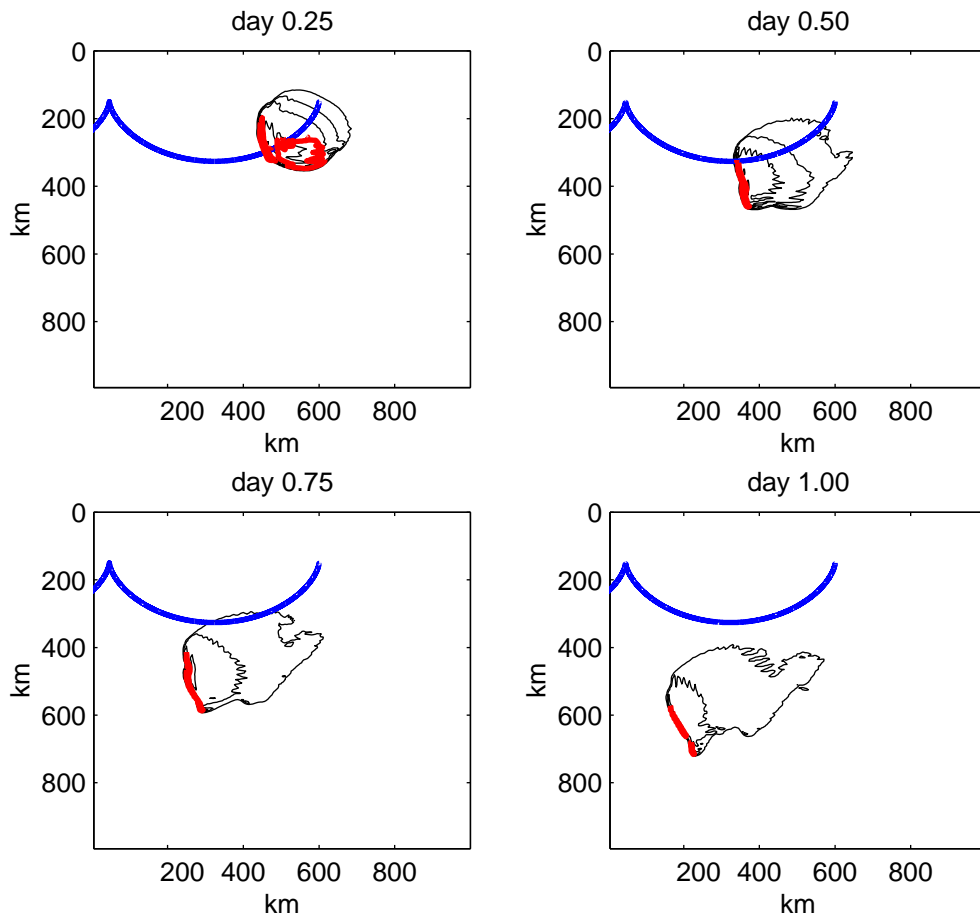


Figure 6: Thickness (contours) and Nof theory (heavy blue line) for day 0.25 (top left), day 0.5 (top right), day 0.75 (bottom left), and day 1.00 (bottom right). Areas with Rossby number greater than 1 are shown with a heavy red contour (stippled in black and white). Same case as Fig. 5, except with bottom friction of 0.001. Contour interval is 10 m.

able to duplicate these assumptions, although we did investigate the effect of viscosity and bottom drag on the solution.

We also found that in some cases, the turbidity current collects into a small, rapidly moving area. The formation of this area is dependent on the Rossby number of the flow. Flows with a large (>1) Rossby number develop this rapidly moving area, while flows with a smaller Rossby number do not. This feature is intriguing, and further study of its development is planned.

5.1 Future work

There are several issues related to the flow of turbidity currents that warrant further exploration. Specifically, several questions remain regarding the formation of the drip region:

1. What is the dependence on model resolution?

To date, we have only run the turbidity current simulations with a horizontal resolution of 5 km. The small scales seen in the drip region indicate that a higher resolution may be necessary to fully resolve the details of the flow in this region.

2. Does the drip appear when other—more appropriate—models are used?

MICOM is intended to model the ocean circulation on the scale of an ocean basin. The extreme conditions (i.e. high velocities and steep height gradients) in the drip region may make the use of MICOM inappropriate for such a simulation. In the simulations shown in Fig. 4, the Froude number of the flow reached a minimum of about 1.8 in the drip region, indicating that the flow is close to a shock wave. Verifying the MICOM results with a shock resolving (i.e. energy and momentum conserving) model would lend credence to the results obtained using MICOM.

3. How does the upper layer influence the dynamics of the current?

Recent papers[8, 9] have shown that the ambient fluid can influence the dynamics of the intruding gravity current. We briefly investigated the role of the depth of the ambient fluid and found little influence on the dynamics of the gravity current. More investigation in this area—including the role of ambient stratification—is warranted.

4. How does entrainment/detrainment affect the dynamics of the turbidity current?

Entrainment and detrainment are major factors in the dynamics of gravity currents[5]. A full study of the dynamics of turbidity currents must include an investigation of the role of entrainment.

6 Acknowledgments

I am greatly indebted to Eric Chassignet for his guidance this summer. He was an excellent mentor in every way and I am grateful to him for the time that he spent with me. I also appreciate conversations with Jim Price throughout the summer. Besides the valuable comments he offered during our conversations, Jim referred me to the paper by Nof[10] which was instrumental in this project. Less directly related to this project, I would like

to thank the staff and visitors of the 2000 GFD program, in particular the organizer, Rick Salmon, and the principal lecturer, Issac Held. Finally, thanks to the other GFD Fellows: Cheryl, Chris, Christos, Giulio, Karen, Lucy, Tivon, and Zhiming. It was a great group to spend a summer with.

References

- [1] J. E. Simpson, "Gravity currents in the laboratory, atmosphere, and ocean," *Ann. Rev. Fluid Mech.* **14**, 213 (1982).
- [2] J. F. Price and M. O. Baringer, "Outflows and deep water production by marginal seas," *Deep-Sea Res.* **33**, 161 (1994).
- [3] R. W. Griffiths, "Gravity currents in a rotating system," *Ann. Rev. Fluid Mech.* **18**, 59 (1986).
- [4] P. C. Smith, "A streamtube model for bottom boundary currents in the ocean," *Deep-Sea Res.* **22**, 853 (1975).
- [5] J. H. Jungclauss and J. O. Backhaus, "Application of a transient reduced gravity plume model to the Denmark Strait Overflow," *J. Geophys. Res.* **99**, 12375 (1994).
- [6] L. Jiang and R. W. Garwood, "A numerical study of three-dimensional dense bottom plumes on a slope," *J. Geophys. Res.* **100**, 18471 (1995).
- [7] L. Jiang and R. W. Garwood, "Three-dimensional simulations of overflows on continental slopes," *J. Phys. Ocean.* **26**, 1214 (1996).
- [8] G. F. Lane-Serff and P. G. Baines, "Eddy formation by dense flows on slopes in a rotating fluid," *J. Fluid Mech.* **363**, 229 (1998).
- [9] G. F. Lane-Serff and P. G. Baines, "Eddy formation by overflows in stratified water," *J. Phys. Ocean.* **30**, 327 (2000).
- [10] D. Nof, "Rotational turbidity flows and the 1929 Grand Banks earthquake," *Deep-Sea Res.* **43**, 1143 (1996).
- [11] J. R. Holton, *An Introduction to Dynamic Meteorology* (Academic Press, ADDRESS, 1992).
- [12] D. B. Haidvogel and A. Beckmann, *Numerical Ocean Circulation Modeling* (Imperial College Press, ADDRESS, 1999).
- [13] P. C. Smith, Ph.D. thesis, Massachusetts Institute of Technology, Cambridge, Mass., 1973.